Seamless Transfer of Renewable-Based Microgrid Between Utility Grid and Diesel Generator

Bhim Singh, *Fellow, IEEE*, Geeta Pathak, *Member, IEEE*, and Bijaya Ketan Panigrahi, *Senior Member, IEEE*

***Abstract*—This paper deals with the renewable energy-based microgrid (MG) to feed the community loads. It has the capability to synchronize with the utility as well as with the diesel generator (DG) set. During healthy grid condition at high renewable power generation and when load demand is less, it feeds power to the grid while at low renewable generation power is taken from the grid. During outage and low renewable power generation, it synchronizes with the DG set to meet the load demand and forms a hybrid microgrid. In islanding, the voltage source converter (VSC) operates in a voltage control mode for realizing a renewable MG and operates in the current control mode for implementing a hybrid MG and switching to the grid-connected mode. An incremental conductance and perturb & observe approaches with a boost converter are implemented for the maximum power extraction of the renewables. A battery bank is connected at the dc link of VSC. The multifunctional MG synchronization and de-synchronization with ac mains/DG set are discussed in conjunction with variety of test results. In this topology, a single bidirectional converter is implemented and controlled using various control algorithms to manage MG power among generation, storage, and load units. A MATLAB/Simulink model is developed for a wind–solar–diesel based MG. Simulated results are validated with test results on a developed laboratory prototype.**

***Index Terms*—Current control, diesel generator (DG), island, microgrid (MG), power quality, synchronization, voltage control.**

I. Introduction

OVER the 28 years period from 2012 to 2040, the worldwide energy demand of marketed energy is expected to expand from 549 quadrillion British thermal units (Btu) in 2012 to 815 quadrillion Btu in 2040, about a 48% increase. Such a significant increase, as reported in [1], is making a deliberation that the renewable and fossil fuel based energy together can make a bridge between demand and supply. Fossil fuels are also in shrinking state due to exhaustive utilization of the resources for the sake of development, and their price has also hiked [2]. As reported in [1], the world energy-related CO_2 emission is expected to increase from 32.2 billion metric tons in 2012 to 43.2 billion metric tons in 2040 with a 34% increase over the projected period. The efforts are made in this area by reducing fossil fuel based generation in [3] and [4] with maximum utilization of the renewables. Renewables are the fastest growing energy sources because of the advancement in power converters [5], [6] and electricity generation at affordable rates [7]. All such scenarios encourage the microgrid research [8]–[10] to provide energy needs to the local loads and interconnection to the main grid. Therefore, control schemes for smooth transfer are important for a microgrid inverter.

Substantial literature on control algorithms for seamless transition of distributed systems and microgrid is available. In [11] and [12], an inverter control is based on current control and voltage control mode for the grid tied and an island operation. A slow synchronization process along with distortion and spikes is observed in load voltages and currents at the time of transition. These shortcomings are eliminated further in [13]. In [13], a phase-locked loop (PLL) based control scheme is implemented for the grid-connected and islanding modes and seamless transitions without having any abnormality. The complete stability analysis on control techniques is also given, and the reactive/linear loads are considered. In [14], an indirect current control technique realized with an inner capacitor voltage loop and external grid current feedback loop is implemented. A rigorous analytical work is done, and smooth transition processes are reported. However, the synchronization process is slow taking almost 18 cycles due to PLL slow angle tracking. In [15] and [16], controllers for seamless transition of microgrid inverters are reported. A universal controller for a three-phase microgrid inverter is also reported for synchronization and islanding processes [15]. Vast analysis and design aspects of microgrid are explained in this paper. Simulation and hardware results are demonstrated with smooth transition on linear loads only. Here, an important feature of microgrid viz. power quality is missing. However, power quality improvement is considered in [16] with simulated results of single-phase microgrid. Controls based on droop concept in [17] are slow during transition, and voltage and current profiles are also poor having distortions. In [18], universal integrated synchronization and control (UISC) is proposed, which is similar to the droop method and also has similar idea of PLL and enhanced phase-locked loop (EPLL) for frequency and phase extraction toward synchronization. Therefore, the single controller is utilized in standalone and grid-tied modes, and the fast transition is possible, which was not reported in droop-based controllers for seamless transition. A detailed stability analysis on UISC is given for standalone and grid-operated modes. In [19], a highly reliable grid synchronization technique based on controller area network communication is proposed

Manuscript received January 15, 2017; revised June 1, 2017 and August 8, 2017; accepted November 14, 2017. Date of publication November 28, 2017; date of current version July 15, 2018. Recommended for publication by Associate Editor M. Molinas. (*Corresponding author: Geeta Pathak.*)

The authors are with the Department of Electrical Engineering, Indian Institute of Technology Delhi, New Delhi 110016, India (e-mail: bsingh@ee.iitd.ac.in; bijayaketan.panigrahi@gmail.com; pathakgita28@gmail.com).

Color versions of one or more of the figures in this paper are available online at http://ieeexplore.ieee.org.

Digital Object Identifier 10.1109/TPEL.2017.2778104

for microgrid seamless transition. It helps various micro units to synchronize accurately with the grid. Though the voltage and current transients and distortions are small, however, the transfer processes are quite slow. In [20], a distributed active synchronization is proposed avoiding high speed communication and synchronization criteria are also derived in detail. To resolve power quality issues, the distortion synchronization control is presented.

In this investigation, renewable-based microgrid synchronization to the grid and a diesel generator (DG) set is considered. Normally, the DG set is kept standby as the focus is on optimum utilization of renewable power and economic utilization of fossil fuels due to fast declining nature of the latter. The DG set is connected under the worst conditions when the renewable generation is very low or nil, the grid is also not available and the battery support is insufficient for the demand. Rest of the time either renewables or the grid supply power to the load. The DG set and the grid are connected to the microgrid through the STS (STS), which toggles between the grid and DG set according to the load requirement and the grid availability. The microgrid topologies described in [21]–[23], deal with the hybrid microgrids with multiple energy resources and ac–dc loads. In these investigations for each topology, numerous bidirectional ac–dc converters and switches are utilized and a converter is used on individual resource.

The topology proposed in this paper includes a three-phase voltage source converter (VSC) to accommodate all dc sources of distributed generation units like wind, solar, and the storage unit at its dc link. This bidirectional converter is capable of converting dc power into ac power, and vice-versa, to provide power balancing by using appropriate control algorithms, for islanded mode with voltage control algorithm (VCA) and the grid/ DG set connected mode with current control algorithm (CCA). The grid or DG set can be connected at point of common coupling (PCC) through STS depending upon the necessity of the load. A manual switch is used to change from the grid mode to DG mode and vice-versa. The synchronization control is also required for the transient free seamless transition between these three modes. This takes corrective action in VSC voltage angle, and when the voltage and angle are under the limit according to [20], the synchronization starts with STS closing and simultaneously the control of VSC changes from VCA to CCA. Substantial literature is available on maximum power point tracking (MPPT) techniques using dc–dc converters, as reported in [24] and [25]. The maximum powers of renewable resources (wind and solar) are extracted using perturb and observe (P&O) method and an incremental conductance (INC) approach as suggested in the literature [26], [27] for the switching of a boost converter. The grid/ DG voltage angle is extracted using EPLL, which is used for phase extraction as in [28]–[30]. The microgrid is multitasking, as in the following.

1) In islanded mode, and it manages the power flow and creates power balance among all the units of microgrid and provides power quality solutions.
2) In grid-tied mode, microgrid VSC feeds power to the grid (grid feeding) or can receive power from the grid (grid operating) depending on the load demand and renewable generation.
3) Under the DG set operating mode when low renewable power generation and the grid outage occur and the battery support is also not available for long duration, the DG set operates and delivers power to the load.

All these mode changes are realized smoothly without having transients in voltages and currents.

The main contributions of this paper are as follows.

1) Modeling and stability analysis of PI controller based VCA during islanding operation is demonstrated. Detailed mathematical framework for CCA of microgrid VSC is developed.
2) Single VSC is implemented for the grid or DG set synchronization to form grid-connected system or hybrid microgrid to serve the community. This VSC is capable of dealing with the renewable generations and the battery storage. Therefore, it reduces the number of converters as compared to the ones normally utilized in microgrids, as in [21]–[23], and thus makes the overall system economic.
3) This microgrid is capable of improving the power quality as per the IEEE 519 standard.
4) During grid availability, control algorithms are capable of synchronizing with the grid, and a transient free fast synchronization takes place within few cycles (4), (5). Smooth and transient free transfer of modes is achieved, which is demonstrated through simulation and test results.
5) Such microgrid synchronizes with DG set and forms a hybrid microgrid when the grid is absent and renewable generation is low. In this way, the DG set is used only for the emergency conditions, saving the fossil fuel, a step toward the economic utilization of conventional sources.
6) The renewable power is utilized to its optimum limit by using the various MPPT techniques.
7) The DG/grid synchronization approach with a single VSC has also not been considered in the past as considered in this paper and is one of the main contributions.

The microgrid model is developed in MATLAB/Simulink using Sim Power Tool box, and simulated results of all three modes are shown in detail. The proposed approach is proved by developing a laboratory prototype and has revealed its multifunctional capabilities with experimental results.

II. Microgrid Configuration

A three-phase hybrid microgrid consisting of two renewable energy resources viz., wind, solar, and a DG set is shown in Fig. 1. Wind and solar generating systems are connected at the dc bus parallel to a battery bank to compensate the system losses and to balance power flow during low generations or during peak demand conditions. The battery stores energy during high renewable generations or delivers during peak load demand. The wind power is generated using a permanent magnet brushless dc generator with a diode bridge rectifier (DBR). This dc power is fed to the boost converter for MPPT. The solar power is also fed to the battery bank through a boost converter. The INC and P&O techniques are used for MPPT. The ac power from the DG set is directly supplied to the ac loads during outage and insufficient renewable generation. A DG set or main grid is attached to the PCC through STS depending on the grid condition. Interfacing

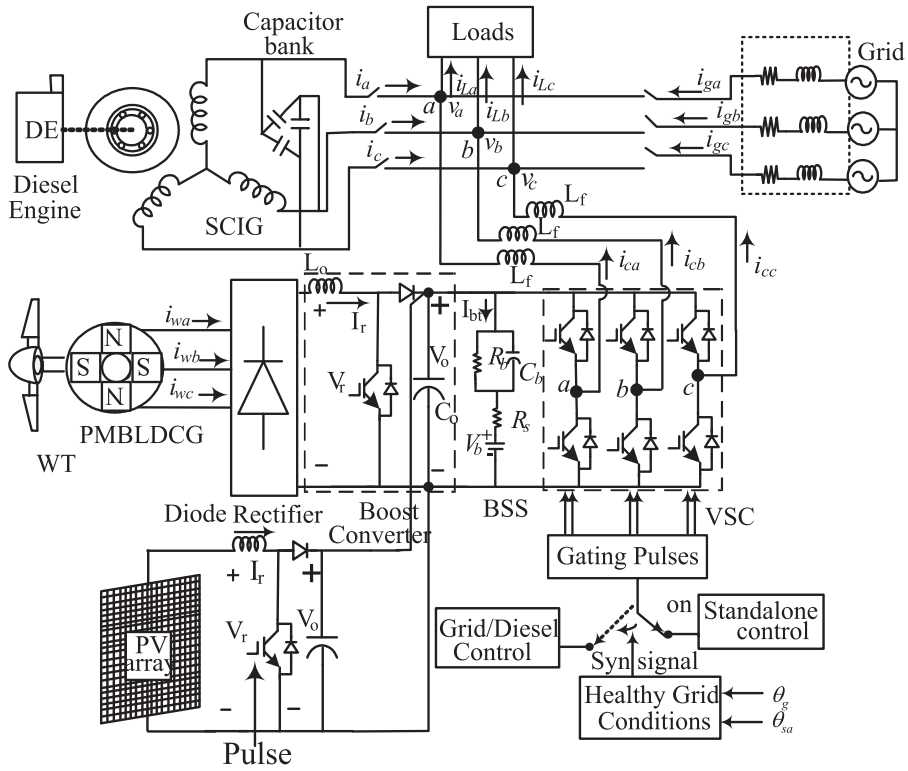

Fig. 1. Schematic diagram of wind-solar-diesel microgrid with utility grid.

inductors (L_f) and *RC* filter are connected at PCC to improve the power quality of the microgrid.

III. Grid Control Strategies for Microgrid Synchronization With Utility Grid/DG

In standalone operation with renewable resources, the VSC operates in a voltage control mode and at grid availability or DG operation, the VSC operates in the current control mode. Hence, the VSC operates with two control algorithms namely VCA and CCA under three modes of operations.

A. Voltage Control Algorithm

Fig. 2 shows the VCA. In this, the reference voltages for an islanded mode are derived as

$$v_{La}^{*} = V_p^{*} \sin(\omega_0 t) \tag{1}$$

$$v_{Lb}^{*} = V_p^{*} \sin\left(\omega_0 t - \frac{2\pi}{3}\right) \tag{2}$$

$$v_{Lc}^{*} = V_p^{*} \sin\left(\omega_0 t + \frac{2\pi}{3}\right) \tag{3}$$

where V_p^{*} and ω_0 are peak reference voltage magnitude and nominal frequency of 50 Hz, respectively.

These reference load voltages (v_{La}^{*}, v_{Lb}^{*}, v_{Lc}^{*}) and sensed load voltages (v_{La}, v_{Lb}, v_{Lc}) are fed to the comparator for generating a voltage error. This voltage error is fed to the proportional integral (PI) controller to achieve the reference load currents (i_{La}^{*}, i_{Lb}^{*}, i_{Lc}^{*}). These reference load currents are compared with sensed load currents (i_{La}, i_{Lb}, i_{Lc}) to generate pulse width modulation (PWM) pulses for the switching of VSC. The block diagram of one phase of VCA is shown in Fig. 2. The PI-controller used in voltage control loop and system stability analysis during a voltage control scheme is depicted in [31] and [32].

Matrix representation of closed-loop transfer functions (A, B) is given here for VCA-based system, which is shown in Fig. 2, as follows, (4) shown at the bottom of the next page, where $A = v_L(\mathrm{s})/v_L*(s)$, $B = v_L(\mathrm{s})/i_L(\mathrm{s})$.

Figs. 3 and 4 illustrate the frequency response and the pole-zero plot of the closed-loop transfer function "A." The frequency response of "A" at power frequency ($\omega = 314$ rad/s) shows 0-dB gain and phase shift is also zero. It states that the output (load voltages-v_{La}, v_{Lb}, v_{Lc}) is almost equal to the input quantity (i.e., reference voltages- v_{La}^{*}, v_{Lb}^{*}, v_{Lc}^{*}). Fig. 4 illustrates the location of poles as $(-4429.996 + 8129.549i)$, $(-4429.996 - 8129.54i)$, -0.00833. All the poles are located on the left-hand side from the origin. Fig. 5 depicts the root locus of open-loop gain of "A," and its gain and phase margins are also calculated as gm = Inf, pm = 57.303312396483690. As these are positive, therefore the system is stable for VCA with PI controller.

B. Indirect CCA

The VSC switching is controlled with the indirect CCA during the grid or DG operating mode, as shown in Fig. 6.

The grid phase voltages can be computed from system line voltages as [33]

$$v_{ga} = \frac{1}{3}\left(2v_{gab} + v_{gbc}\right) \tag{5}$$

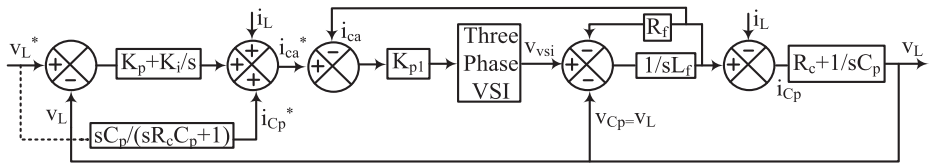

Fig. 2. Block diagram for one phase of VCA of microgrid.

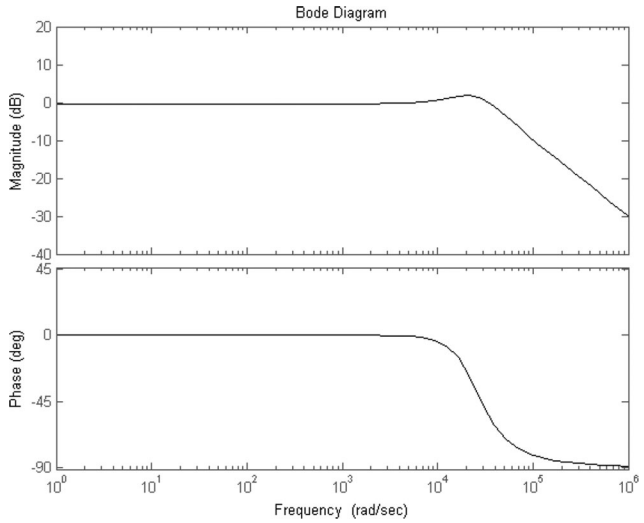

Fig. 3. Frequency response of VCA for a closed-loop transfer function ($v_L(s)/v_L^*(s)$).

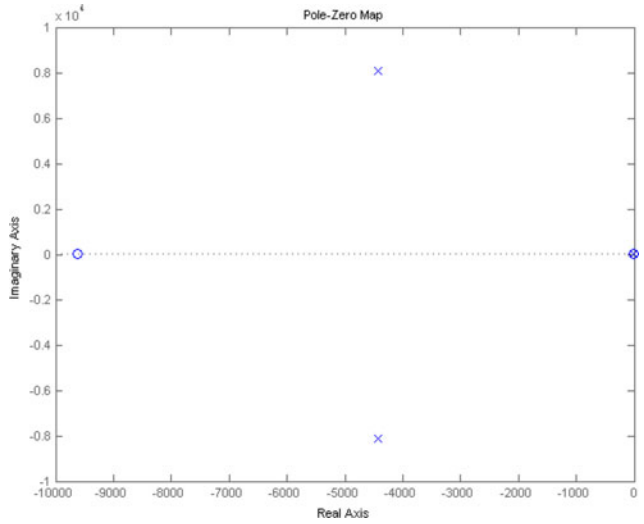

Fig. 4. Pole-zero map for the system voltage control stability.

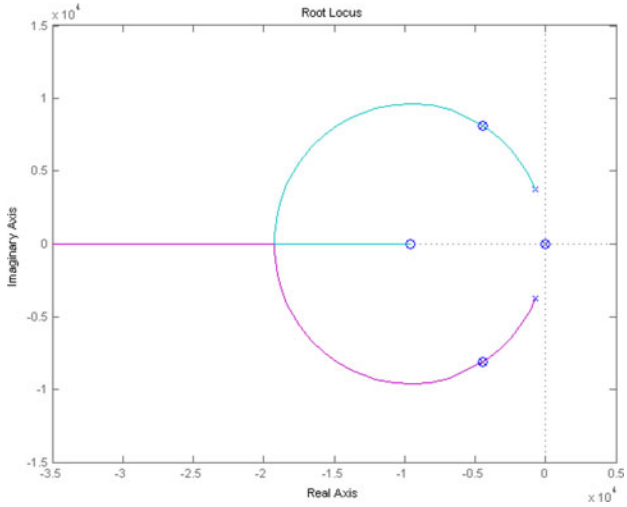

Fig. 5. Root locus of open-loop gain of transfer function A.

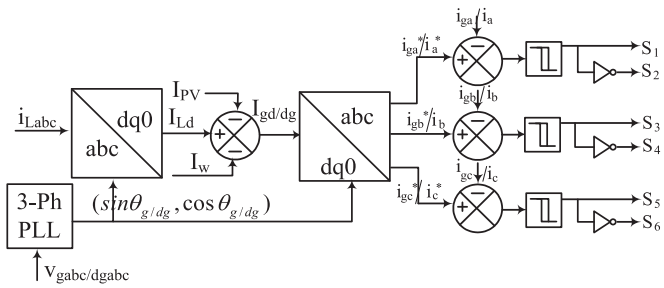

Fig. 6. Current control for grid tied/DG operation.

$$v_{gb} = \frac{1}{3}\left(-v_{gab} + v_{gbc}\right) \tag{6}$$

$$v_{gc} = \frac{1}{3}\left(-v_{gab} - 2v_{gbc}\right). \tag{7}$$

The terminal voltage amplitude (V_t) is derived from the phase voltages as

$$V_{gt} = \sqrt{\left(2\left(v_{ga}^2 + v_{gb}^2 + v_{gc}^2\right)/3\right)}. \tag{8}$$

$$[v_L] = [A\ B]\begin{bmatrix} v_L^* \\ i_L \end{bmatrix}$$

$$A = \frac{s^2(K_pK_{p1}R_cC_p + K_{p1}C_p) + s(K_iK_{p1}R_cC_p + K_pK_{p1}) + K_{p1}K_i}{s^3(L_fC_p) + s^2\{R_cC_p(1+K_pK_{p1}) + C_p(R_f+K_{p1})\} + s\{(1+K_pK_{p1}) + K_iK_{p1}R_cC_p\} + K_{p1}K_i}$$

$$B = \frac{s^3(L_fR_cC_p) + s^2\{L_f + R_cC_p(R_f+K_{p1})\} + s(R_f+K_{p1})}{s^3(L_fC_p) + s^2\{R_cC_p(1+K_pK_{p1}) + C_p(R_f+K_{p1})\} + s\{(1+K_pK_{p1}) + K_iK_{p1}R_cC_p\} + K_{p1}K_i} \tag{4}$$

The amplitude of the DG terminal voltages are calculated in the similar manner. The load currents in the three phases are converted into the *d-q-0* frame using the Park's transformation as follows [34], [35]:

$$\begin{bmatrix} i_{Ld} \\ i_{Lq} \\ i_{L0} \end{bmatrix} = \frac{2}{3} \begin{bmatrix} \cos\theta_g & -\sin\theta_g & \frac{1}{2} \\ \cos\left(\theta_g - \frac{2\pi}{3}\right) & -\sin\left(\theta_g - \frac{2\pi}{3}\right) & \frac{1}{2} \\ \cos\left(\theta_g + \frac{2\pi}{3}\right) & \sin\left(\theta_g + \frac{2\pi}{3}\right) & \frac{1}{2} \end{bmatrix} \begin{bmatrix} i_{La} \\ i_{Lb} \\ i_{Lc} \end{bmatrix}. \tag{9}$$

After passing through the low-pass filter, the active component of the load current (i_{Ld}) is considered as I_{Ld}. The reference active components of source (grid/ DG) are derived as

$$I_{Tp} = (I_{Ld} - I_w - I_{\rm PV}) \tag{10}$$

where the active component of wind current I_w is calculated as

$$I_w = \frac{P_w}{3V_t}. \tag{11}$$

The active component of solar PV current $I_{\rm PV}$ is calculated as

$$I_{\rm PV} = \frac{P_{\rm PV}}{3V_t} \tag{12}$$

where P_w, $P_{\rm pv}$ and V_t are the wind power and PV power after MPPT, and the amplitude of terminal voltage, respectively.

Using inverse Park transform, reference grid currents ($i^*_{ga,}$ i^*_{gb}, and i^*_{gc},) are generated

$$i^*_{ga} = \frac{2}{\sqrt{3}}(I_d \sin\theta_g + I_q \cos\theta_g) \tag{13}$$

$$i^*_{gb} = \frac{2}{\sqrt{3}}[I_d \sin\left(\theta_g - 2\pi/3\right) + I_q \cos(\theta_g - 2\pi/3)] \tag{14}$$

$$i^*_{gc} = \frac{2}{\sqrt{3}}[I_d \sin\left(\theta_g + 2\pi/3\right) + I_q \cos(\theta_g + 2\pi/3)] \tag{15}$$

where $I_d = I_{gt}$ and $I_q = 0$.

The sensed grid currents ($i_{ga,}$ i_{gb}, and i_{gc}) are compared with these reference grid currents ($i^*_{ga,}$ $i^*_{gb,}$ and i^*_{gc},) to generate VSC switching pulses. The hysteresis PWM is used for switching of VSC. In this, hysteresis comparators are used to impose a hysteresis band around the reference current. It confines current ripples in the hysteresis band and keeps small variation of the sensed current and remains nearly sinusoidal. The similar methodology is used for reference DG currents generation.

C. *Synchronization Control for VSC Angle Correction*

The grid and DG set in-phase ($\sin\theta_g$, $\sin\theta_{dg}$) and quadrature ($\cos\theta_g$, $\cos\theta_{dg}$) phase angles are generated using EPLL, as shown in Fig. 7(a). The angle error is estimated as

$$\sin(\theta_g - \theta_{sa}) \approx (\theta_g - \theta_{sa}) = \Delta\theta. \tag{16}$$

The PI controller produces an increment in the frequency ($\Delta\omega$) output of an isolated system before synchronization, as shown in Fig. 7(b). The correction is added into the actual value of VSC voltage angle (θ_{sa}) to update the load angle toward the grid/DG voltage angle (θ_g/θ_{dg}).

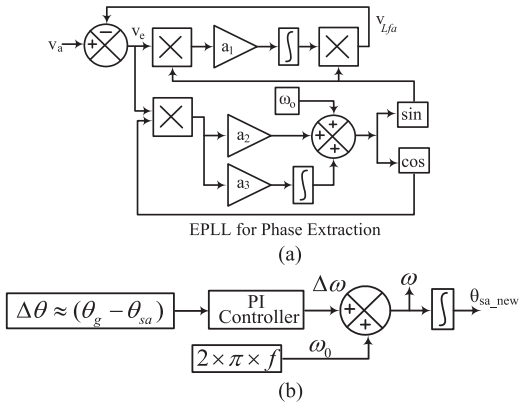

Fig. 7. (a) Phase angle extraction. (b) Phase angle matching using a PI controller.

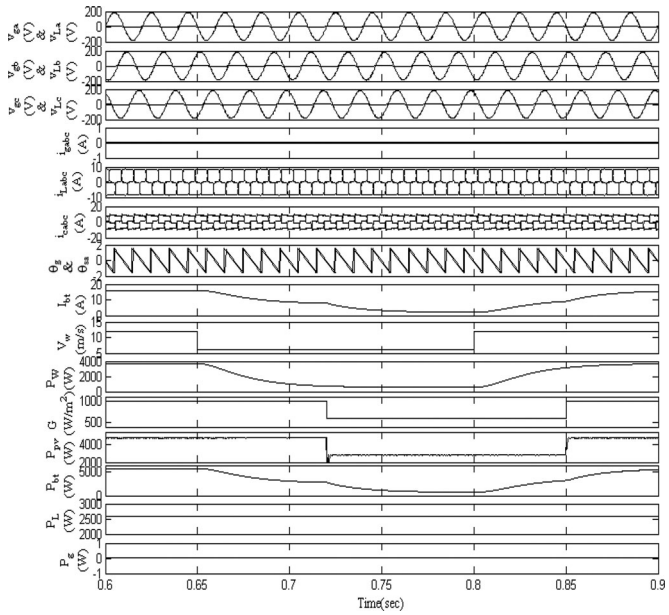

Fig. 8. Standalone mode of operation of microgrid under nonlinear load.

IV. Simulated Results

This section includes the simulation results with standalone, grid-tied, and DG set modes with synchronization and desynchronization processes. The VCA and CCA of microgrid are used during different modes of operation and for smooth and transient free mode switching among VSC, the grid and DG set. The microgrid performance is observed under different scenarios as in standalone operation, grid feeding mode, and DG operating mode to feed the loads with reduced renewable generation.

A. *Island Operation of Microgrid at Nonlinear Load*

In an island mode, the microgrid supplies ac power to the load from dc generation of renewable energy resources, which is converted into ac power using a VSC. Fig. 8 depicts the microgrid operation in an isolated mode with renewable generation.

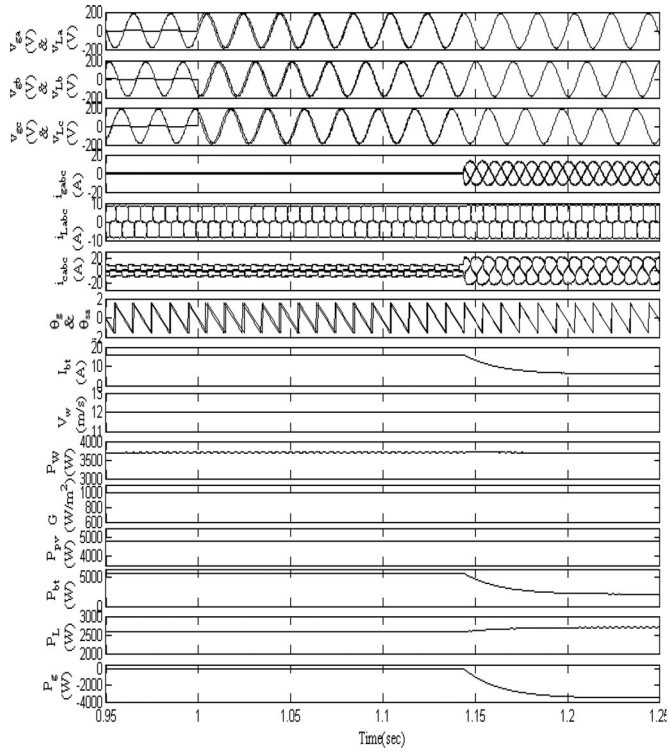

Fig. 9. Synchronization of microgrid to the grid under nonlinear load.

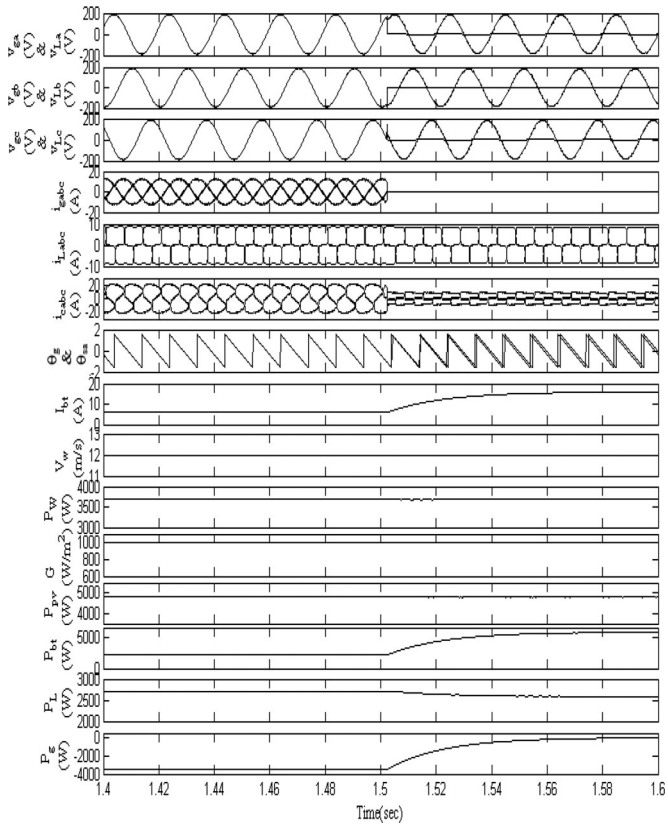

Fig. 10. De-synchronization of microgrid from grid under nonlinear load.

The load voltages ($v_{La},\ v_{Lb},\ v_{Lc}$) are sinusoidal and maintained constant with the fixed load demand ($P_L,\ i_{Labc}$). The grid voltages and currents ($v_{gabc},\ i_{gabc}$) are absent due to the grid outage. Due to the variation in wind speed and solar insolation, the wind (P_w) and solar power (P_{pv}) variations are seen. During the wind and solar power reduction, the battery storage system justifies its role of being in the microgrid. It provides the power balance and fulfills the load demand during low or nil renewable generations. Therefore, the charging current (I_{bt}) and battery power (P_{bt}) are reduced with the wind speed and insolation decrease. The grid power (P_g) is zero. The VSC and grid voltage phase angles (θ_{sa} & θ_g) are at different values. VSC is feeding the nonlinear load, therefore, VSC currents (i_{cabc}) are also nonlinear.

B. Performance During Grid Synchronization and De-Synchronization Process

During grid availability, the microgrid synchronization control operates and STS closes to synchronize the microgrid to the ac mains. Simultaneously, VSC control changes from VCA to CCA. The synchronization process of the renewable microgrid to the utility grid is shown in Fig. 9 at nonlinear load. The grid appears when the grid voltages (v_{gabc}) are available at $t = 1$ s. The synchronization of the microgrid VSC to the utility grid takes place within few cycles. At $t = 1.15$ s, when the voltage magnitudes and angles are within the limit according to [18], the STSs are closed and the synchronization takes place. Therefore, the grid currents and power ($i_{gabc},\ P_g$) are appeared. The negative power is the sign that excess renewable power after supplying to the load is fed to the grid. The control algorithm switches from the VCA to CCA, therefore VSC currents (i_{cabc}) are also changed accordingly. The grid and VSC voltages angles (θ_g & θ_{sa}) are synchronized. As the wind–solar generation and the load demand are fixed, the battery power and current are reduced as now the power is fed to the grid rather than feeding to the storage. The VSC currents and P_g are increased as VSC is feeding the remaining power to the grid. The de-synchronization process appears when the grid outage occurs. In Fig. 10 at $t = 1.5$ s, the grid is unavailable, therefore the grid currents and power disappear and become zero. At the same instant, the control is changed from the grid-connected to the island mode. Therefore, the VSC currents are also changed and excess power is stored into the battery bank. The changeover between an island mode to the grid-tied mode, and vice-versa, is realized smoothly using the synchronization control for closing/opening of the STS without having transients.

C. Performance During DG Synchronization

At the time of outage, the switch is connected from the grid to the DG set to feed the local load requirements. The generator is synchronized to the VSC without having transients in voltages and currents of loads and source ($v_{sabc},\ v_{Labc}$), as shown in Fig. 11. The source currents (i_{sabc}) are maintained constant and sinusoidal. The phase angles are synchronized. At $t = 2$ s, the DG set along with a battery feeds powers during less or nil renewable power generation. It can be seen that with the reduction in wind speed and insolation level when the wind and

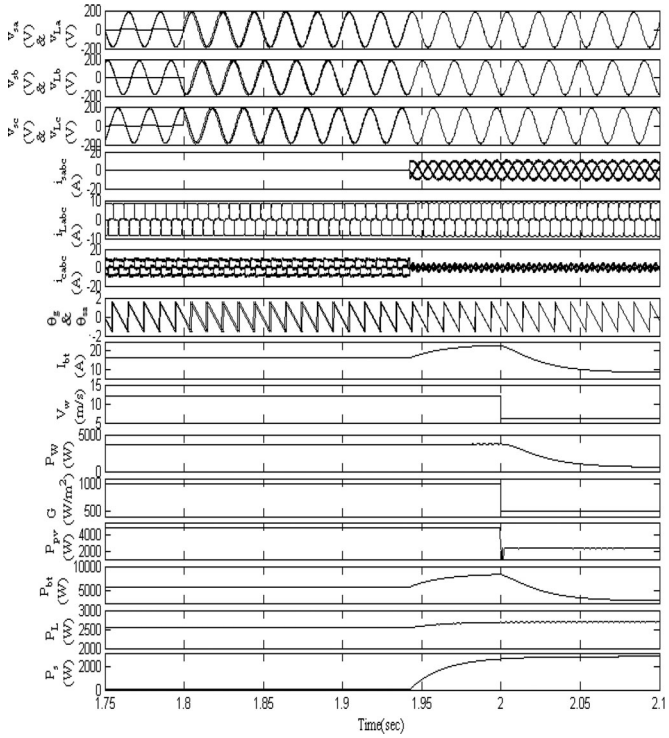

Fig. 11. DG synchronization with wind–solar microgrid.

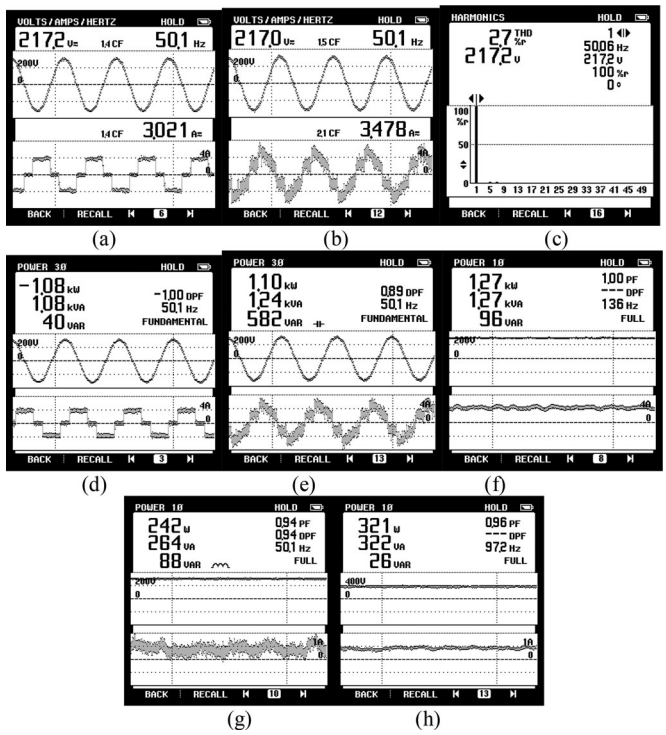

Fig. 12. Steady-state performance of standalone microgrid. (a) Load current (i_{Lc}) and V_{Lab}. (b) VSC current (i_{cc}) and V_{Lab}. (c) Harmonic content of load voltage. (d) P_L. (e) $P_{\rm VSC}$. (f) Solar power (P_{pv}). (g) Wind power (P_w). (h) Stored power (P_{bt}).

the solar PV powers are decreased, the battery current and power are reduced to provide the power leveling. DG set provides its rated power to the load demand. With the grid recovery, DG set is disconnected and the battery supports the microgrid and further the microgrid synchronizes to the utility.

V. Experimental Performance of Wind-Based Microgrid at Nonlinear Load

A prototype is developed in the laboratory to study the wind–solar–diesel microgrid performance in detail during steady-state and dynamic conditions at nonlinear load. The microgrid performance is observed under steady state in different scenarios as standalone mode of renewable-based microgrid, grid-feeding mode, and DG set feeding to the loads with low renewable generations. The Hall effect current sensors and voltage sensors are used to sense the PCC voltages and currents. The control algorithm is implemented on a DSP-dSPACE 1103. A digital storage oscilloscope- DSO (Agilent make- DSO-7014A) and a power analyzer (Fluke- 43B) are used to record the test results at nonlinear loads.

A. Steady-State Performance of Microgrid Under Various Modes of Operation

Steady-state performance of wind–solar–diesel microgrid in islanded, grid-tied, and DG set operated modes, are detailed under this section.

1) Performance Under Island Mode at Nonlinear Loads: The steady-state performance of the renewable microgrid during islanded mode with sufficient renewable power generation and the grid outage is shown in Fig. 12 at nonlinear load. The load current (i_{Lc}) and VSC current (i_{cc}) with line voltage (v_{Lab}) are shown in Fig. 12(a) and (b). The voltage profile is sinusoidal with its total harmonic distortion (THD) less than 5%, as depicted in Fig. 12(c). The load demand (P_L) and VSC power are depicted in Fig. 12(d) and (e). It is clear that the load demand is met through the VSC power by converting dc renewable power into ac power. The wind generation (P_w) and solar power generation ($P_{\rm PV}$) are shown in Fig. 12(f) and (g), and the excess renewable power after feeding the load is stored into the battery bank, as shown in Fig. 12(h).

2) Performance Under Grid-Tied Mode at Nonlinear Loads: During the grid-connected mode, the microgrid is feeding power to the utility grid when the load demand is less and generation is high. The VSC is operating in the current control mode, and test results are demonstrated in Fig. 13 at nonlinear load (three-phase DBR with inductive load). Fig. 13(a)–(c) show the grid current, load current, and VSC current of phase "c" with PCC voltage (v_{ab}). The PCC voltage, load current, and grid current THDs are demonstrated in Fig. 13(d) and (f). The harmonic contents of grid feeding powers are very small and as per IEEE 519 standard, which do not inject harmonics in the grid. The microgrid power scenario is depicted in Fig. 13(g)–(l). The grid is fed with a $P_g = 3.02$ kW, and the load demand is ($P_L = 0.797$ kW). These powers are coming from VSC ($P_{\rm vsc} = 3.9$ kW). It is understood that VSC is converting the dc power of renewables and the battery into the ac power to feed the load and the grid. It is demonstrated in Fig. 13(j)–(l) as the total renewable power is

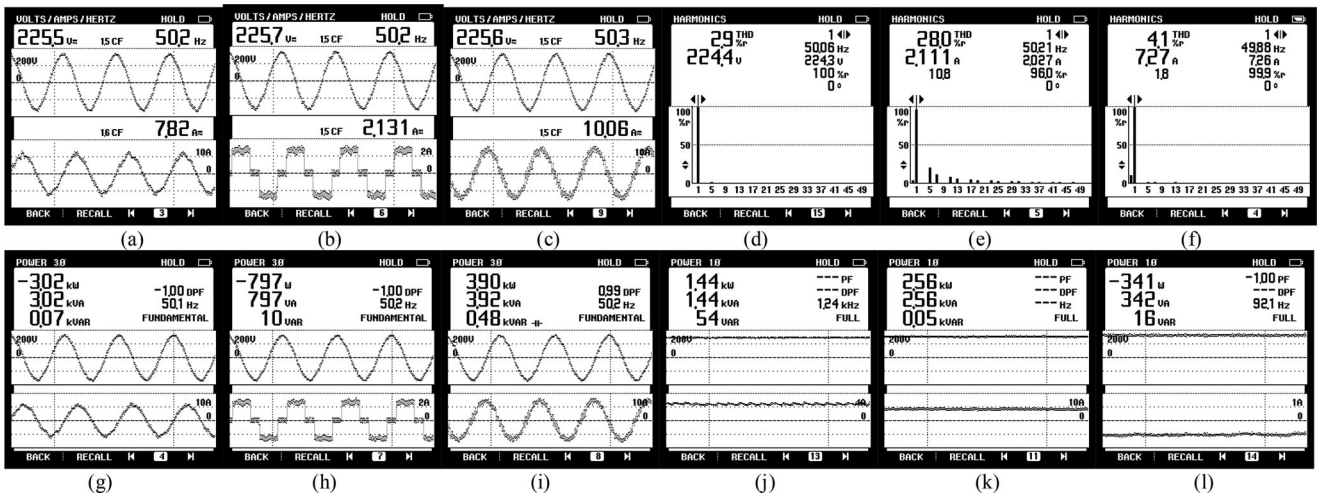

Fig. 13. Performance of microgrid during grid-connected mode. (a)–(c) Grid current (i_{ga}), Load current (i_{La}), VSC current (i_{ca}) with V_{gab}. (d)–(f) Harmonic content of line voltage, load current, and grid current. (g) P_g. (h) P_L. (i) P_{vsc}. (j) Wind power (P_w). (k) Solar power (P_{pv}). (l) P_{bt}.

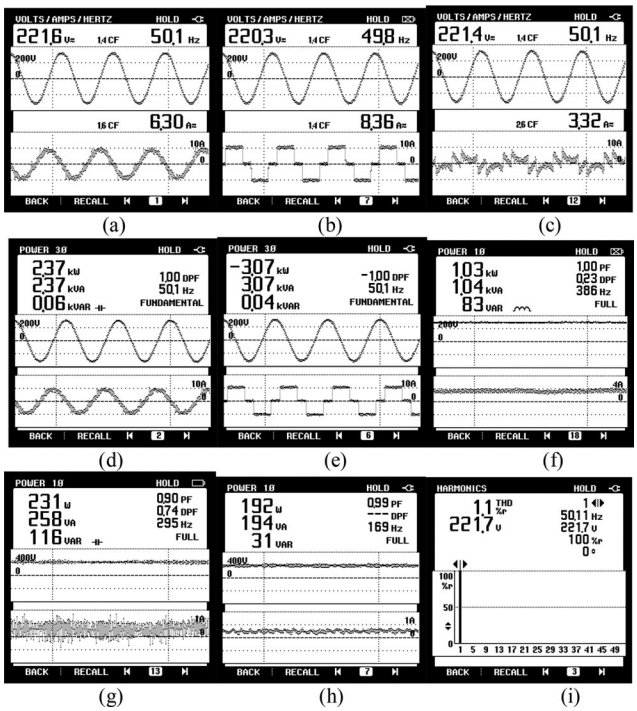

Fig. 14. Performance of hybrid microgrid. (a) Source current (i_c) and V_{Lab}. (b) Load current (i_{Lc}) and V_{Lab}. (c) VSC current (i_{cc}) and V_{Lab}. (d) P_s. (e) P_L. (f) Solar power (P_{pv}). (g) Wind power (P_w). (h) Battery power (P_{bt}). (i) Harmonic content of load voltage.

from solar and wind powers ($P_w + P_{pv} = 2.56 + 1.44 = 4\,\text{kW}$) and the battery power ($P_{bt} = 0.341\,\text{kW}$). Some power is wasted in the loss in different components. The system works well with healthy voltage conditions and power balance.

3) Performance Under DG Operated Mode With Renewable Power Generation: This scenario is considered during outage when the load demand is high and the renewable power generation is not sufficient or nil to feed the load demand, therefore, the DG is providing the deficit power to the loads. Test results of the DG-operated microgrid are considered in Fig. 14. The source current (i_c), nonlinear load current (i_{Lc}), and VSC currents (i_{cc}) with PCC voltage (v_{ab}) are shown in Fig. 14(a)–(c). The source (DG) power and load demand are depicted in Fig. 14(d) and (e), where the load demand is fed by the source and the battery storage. The wind and solar generations are utilized to feed the load demand, and excess power is stored into the battery bank and exhausted in the system losses, as shown in Fig. 14(f)–(h). The voltage profile shown in Fig. 14(i) is with a THD below 5%, which is within an IEEE 519 standard limit. PCC source voltages and currents of hybrid microgrid are sinusoidal. The microgrid control is capable of improving power quality and power balance between loads and generators.

B. Dynamic Performance of Microgrid

Dynamic performance of the microgrid is implemented with the synchronization and desynchronization from the utility grid. Other scenario is considered with DG synchronization and changeover between grid and DG.

1) Performance During Grid Synchronization and De-Synchronization Process: The smooth transition of VSC control between the grid-tied and island modes is shown in Fig. 15. Fig. 15(a) shows the grid appearance with voltage v_{gab} and the grid synchronizes after few cycles (less than 10) and the grid current (i_{ga}) appears. Fig. 15(b) shows the de-synchronization of the microgrid with the grid voltage and grid current being absent. The load voltage (v_{Lab}) and current (i_{La}) are maintained constant without having any spike. Fig. 15(c) illustrates the grid currents (i_{ga}) with the grid and load voltage angles (θ_g & θ_{sa}) during grid synchronization. They become same under synchronization.

2) Microgrid Dynamics With Wind Speed Variation and Insolation Change: The microgrid feeds the excess renewable power to the grid. The extreme conditions when wind and solar energy both are absent and the load demand is maintained, power comes from the grid to feed the loads, as shown in Fig. 16(a). Grid current (i_{ga}) changes its phase as power flow direction is changed. The dc-link voltage (V_o), battery current (I_{bt}), wind speed in terms of boost converters input current for wind (I_w),

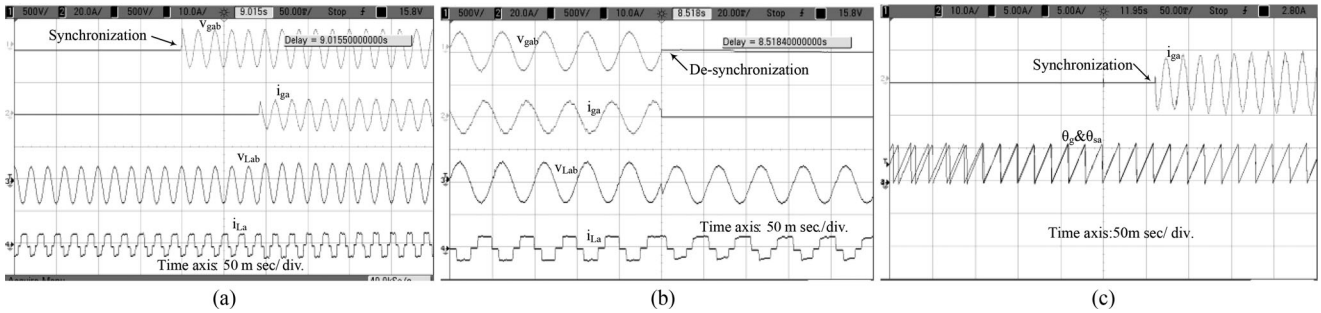

Fig. 15. Synchronization and de-synchronization processes at nonlinear loads: (a) and (b) $v_{ga},\ I_{ga},\ v_{La},\ i_{La}$. (c) $i_{ga},\ \theta_g,\ \theta_{sa}$..

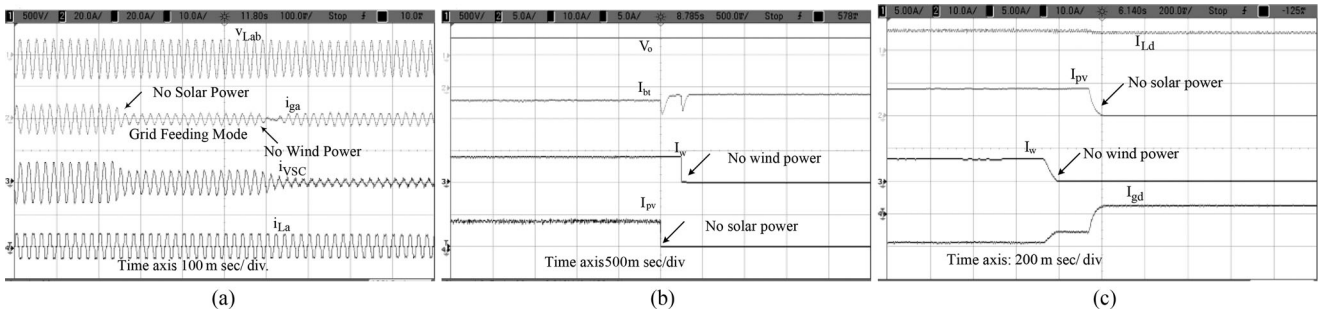

Fig. 16. Dynamic performance of microgrid with wind speed and insolation variation under nonlinear loads. (a) $v_{Lab},\ i_{ga},\ i_{VSC}, i_{La}$, (b) $V_o,\ I_{bt},\ I_w,\ I_{pv}$, (c) $I_{Ld},\ I_{pv}, I_w,\ I_{gd}$.

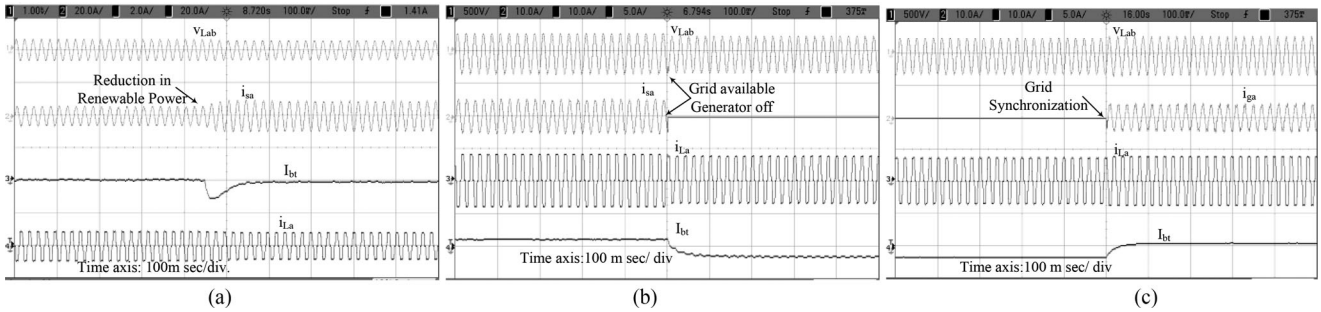

Fig. 17. Performance of hybrid microgrid and synchronization process at nonlinear loads: (a) $v_{Lab},\ i_{sa},\ I_{bt},\ i_{La}$; (b) $v_{Lab},\ i_{sa},\ i_{La},\ I_{bt}$; (c) $v_{Lab},\ i_{ga},\ i_{La},\ I_{bt}$.

and input current for PV (I_{PV}) are shown in Fig. 16(b). Due to the absence of wind and solar powers, the grid provides power to the load, which is fixed. Therefore, the battery discharging current is reduced (as power transfer is reduced) for maintaining the dc-link voltage only. The battery absorbs the sudden deficiency in power, discharges momentarily to provide power balance during wind and solar power variation. Internal parameters of load active component (I_{Ld}), wind component (I_w), solar component (I_{pv}), and active component to feed the grid (I_{gd}) are shown in Fig. 16(c). I_{Ld} is fixed as load demand is constant and with the reduction in wind and solar active power components, the grid component changed its direction and it becomes positive. It shows that with variation in power generation, CCA is capable of maintaining power balance among the units without having interruption in the load demand.

3) Performance During Diesel Generator Dynamics (H-MG): The hybrid microgrid scenarios are considered with sudden reduction in renewable generations. Fig. 17(a) depicts the increase in source (DG current), which is increased due to power reduction from VSC as renewable power is decreased, and DG provides the deficit power to fulfil the demand. DG takes few milliseconds to increase the power, at that time battery supports the system.

Fig. 17(b) and (c) illustrate the change over from DG to the grid. The outage is clear, the grid is available in healthy state, therefore, the DG must be disconnected. It is disconnected from the microgrid, simultaneously the battery and renewables come in action to feed the load demand in the voltage control mode. Therefore, battery discharging current (I_{bt}) is increased, as depicted in Fig. 17(b). In Fig. 17(c), the grid is synchronized with the microgrid and the power is delivered from the grid in terms of grid current (i_{ga}). At the synchronization, the battery current again comes back to its normal position from the discharging state. This demonstrates the microgrid capability as a hybrid MG with a fuel saving approach when the outage is cleared and renewable power generation is increased.

VI. Conclusion

A hybrid microgrid of wind–solar–diesel has been modeled in MATLAB/Simulink. Moreover, its prototype is developed in the laboratory to investigate the microgrid performance under variety of modes as standalone renewable power generation, grid-tied operation of renewable resources, and DG and renewable power (H-MG). The microgrid functions satisfactorily during the islanded mode, the grid-tied mode, and the DG-operated mode and provides the transient free responses during synchronization and de-synchronization processes at grid synchronization and DG set operated synchronization. The VSC switches between voltage control and current control modes smoothly. The synchronization control is very efficient during closing/opening of STS such that no transients are introduced in voltages and currents at synchronization and during islanding process. Mathematical and analytical approaches of control algorithms are considered. The VSC control algorithms have enhanced the power quality as per IEEE standard 519 and power balancing. Single VSC is implemented among dc power units (wind, solar PV, and storage), grid/DG, and nonlinear load. This microgrid makes the overall system economic by reducing the number of converters for individual units of wind, solar PV array, storage, and DG set. The fossil fuel consumption is on the economic way, and is used only when the microgrid renewable generation units are unable to generate renewable power and at the same time outage persists. Such microgrid can serve the purpose of optimum utilization of renewable resources and economic consumption of diesel, especially for the places where the grid outage is frequent.

Appendices

A. PMBLDCG (Permanent Magnet Brushless dc Generator): Three Phase, 3.7 kW, 230 V, 1500 rpm, 13.9 A, 50 Hz.

B. SCIG (Squirrel Cage Induction Generator): Three Phase, 3.7 kW, 230 V, 1430 rpm, 13 A, 50 Hz.

C. Solar PV Array simulator: 2.5 kW, open circuit voltage of PV array (V_{oc}) = 362 V, Short Circuit Current (I_{sc}) = 8.31 A, $V_{mp} = 311.75$ V, $I_{mp} = 7.88$ A, $P_{mp} = 2.456$ kW.

D. Battery bank- $V_b = 360$ V $C_b = 1125$ F, $R_b = 10\,\text{k}\Omega$, Rs = 0.1.

E. Interfacing Inductance $L_f = 3.5$ mH, Ripple Filter Capacitance $C_P = 10\,\mu$F, Resistance $R_c = 5\,\Omega$.

F. Gains for voltage PI controller in VCA: kp = 5, and ki = 0.05.

G. Gains of PI controller for angle control: kp = 1.6, & ki = 0.1.

H. Three-Phase ac grid line 230 V, 50 Hz, dc-link voltage 400 V, dc-link Capacitance = 1600 μF.

Acknowledgment

The authors thank the Department of Science and Technology (DST), Government of India, for sponsoring this project "RP02979—Reliable and Efficient Systems for Community Energy Solution—RESCUES" as an Indo-UK joint research project.

References

[1] J. Conti *et al.*, "International energy outlook," U.S. Energy Inf. Admin., Washington, DC, USA, May 2016.
[2] N. Bauer *et al.*, "Global fossil energy markets and climate change mitigation: an analysis with REMIND," *Climatic Change*, pp. 1–14, 2013.
[3] M. Arriaga, C. A. Caizares, and M. Kazerani, "Long-term renewable energy planning model for remote communities," *IEEE Trans. Sustain. Energy*, vol. 7, no. 1, pp. 221–231, Jan. 2016.
[4] W. M. Lin, C. M. Hong, and C. H. Chen, "Neural-Network-based MPPT control of a stand-alone hybrid power generation system," *IEEE Trans. Power Electron.*, vol. 26, no. 12, pp. 3571–3581, Dec. 2011.
[5] F. Blaabjerg, Y. Yang, and K. Ma, "Power electronics - key technology for renewable energy systems—Status and future," in *Proc. 3rd Int. Conf. Elect. Power Energy Convers. Syst.*, Istanbul, Turkey, 2013, pp. 1–6.
[6] B. K. Bose, "Global energy scenario and impact of power electronics in 21st century," *IEEE Trans Ind. Electron.*, vol. 60, no. 7, pp. 2638–2651, Jul. 2013.
[7] M. Taylor, K. Daniel, A. Ilas, and E. Y. So, "Renewable power generation costs in 2014" International Renewable Energy Agency, Abu Dhabi, United Arab Emirates, Jan. 2015.
[8] X. Lu, J. M. Guerrero, K. Sun, J. C. Vasquez, R. Teodorescu, and L. Huang, "Hierarchical control of parallel AC-DC converter interfaces for hybrid microgrids," *IEEE Trans. Smart Grid*, vol. 5, no. 2, pp. 683–692, Mar. 2014.
[9] Y. Deng, Y. Tao, G. Chen, G. Li, and X. He, "Enhanced power flow control for grid-connected droop-controlled inverters with improved stability," *IEEE Trans. Ind. Electron.*, vol. 64, no. 7, pp. 5919–5929, Jul. 2017.
[10] P. C. Loh, D. Li, Y. K. Chai, and F. Blaabjerg, "Autonomous operation of hybrid microgrid with AC and DC subgrids," *IEEE Trans. Power Electron.*, vol. 28, no. 5, pp. 2214–2223, May 2013.
[11] D. S. Ochs, B. Mirafzal, and P. Sotoodeh, "A method of seamless transitions between grid-tied and stand-alone modes of operation for utility-interactive three-phase inverters," *IEEE Trans. Ind. Appl.*, vol. 50, no. 3, pp. 1934–1941, May/Jun. 2014.
[12] M. Ranjbar, H. Ebrahimirad, S. Mohaghegh, and A. Ghaleh, "Seamless transfer of three-phase grid-interactive microturbine inverter between grid-connected and stand-alone modes," in *Proc. 19th Iranian Conf. Elect. Eng.*, Tehran, Iran, 2011, pp. 1–1.
[13] T. V. Tran, T. W. Chun, H. H. Lee, H. G. Kim, and E. C. Nho, "PLL-based seamless transfer control between grid-connected and islanding modes in grid-connected inverters," *IEEE Trans. Power Electron.*, vol. 29, no. 10, pp. 5218–5228, Oct. 2014.
[14] Z. Liu and J. Liu, "Indirect current control based seamless transfer of three-phase inverter in distributed generation," *IEEE Trans. Power Electron.*, vol. 29, no. 7, pp. 3368–3383, Jul. 2014.
[15] M. Karimi-Ghartemani, S. A. Khajehoddin, P. Piya, and M. Ebrahimi, "Universal controller for three-phase inverters in a microgrid," *IEEE J. Emerg. Sel. Topics Power Electron.*, vol. 4, no. 4, pp. 1342–1353, Dec. 2016.
[16] A. Micallef, M. Apap, C. Spiteri-Staines, and J. M. Guerrero, "Single-phase microgrid with seamless transition capabilities between modes of operation," *IEEE Trans. Smart Grid*, vol. 6, no. 6, pp. 2736–2745, Nov. 2015.
[17] J. Kim, J. M. Guerrero, P. Rodriguez, R. Teodorescu, and K. Nam, "Mode adaptive droop control with virtual output impedances for an inverter-based flexible AC microgrid," *IEEE Trans. Power Electron.*, vol. 26, no. 3, pp. 689–701, Mar. 2011.
[18] M. Karimi-Ghartemani, "Universal integrated synchronization and control for single-phase DC/AC converters," *IEEE Trans. Power Electron.*, vol. 30, no. 3, pp. 1544–1557, Mar. 2015, doi: 10.1109/TPEL.2014.2304459.
[19] S. S. Thale and V. Agarwal, "Controller area network assisted grid synchronization of a microgrid with renewable energy sources and storage," *IEEE Trans. Smart Grid*, vol. 7, no. 3, pp. 1442–1452, May 2016.
[20] F. Tang, J. M. Guerrero, J. C. Vasquez, D. Wu., and L. Meng, "Distributed active synchronization strategy for microgrid seamless reconnection to the grid under unbalance and harmonic distortion," *IEEE Trans. Smart Grid*, vol. 6, no. 6, pp. 2757–2769, Nov. 2015.
[21] C. Wang, X. Li, L. Guo, and Y. W. Li, "A nonlinear-disturbance-observer-based DC-bus voltage control for a hybrid AC/DC microgrid," *IEEE Trans. Power Electron.*, vol. 29, no. 11, pp. 6162–6177, Nov. 2014.
[22] F. Nejabatkhah and Y. W. Li, "Overview of power management strategies of hybrid AC/DC microgrid," *IEEE Trans. Power Electron.*, vol. 30, no. 12, pp. 7072–7089, Dec. 2015.

[23] Y. Xia, Y. Peng, M. Yu, and W. Wei, "Distributed coordination control for multiple bidirectional power converters in a hybrid AC/DC microgrid," *IEEE Trans. Power Electron.*, vol. 36, no. 6, pp. 4949–4959, Jun. 2017.
[24] S. Lyden and M. E. Haque, "A simulated annealing global maximum power point tracking approach for PV modules under partial shading conditions," *IEEE Trans. Power Electron.*, vol. 31, no. 6, pp. 4171–4181, Jun. 2016.
[25] J. C. Y. Hui, A. Bakhshai, and P. K. Jain, "An energy management scheme with power limit capability and an adaptive maximum power point tracking for small standalone PMSG wind energy systems," *IEEE Trans. Power Electron.*, vol. 31, no. 7, pp. 4861–4875, Jul. 2016.
[26] Z. M. Dalala, Z. U. Zahid, and L. Jih-Sheng, "New overall control strategy for small-scale WECS in MPPT and stall regions with mode transfer control," *IEEE Trans. Energy Convers.*, vol. 28, no. 4, pp. 1082–1092, Dec. 2013.
[27] M. A. Elgendy, B. Zahawi, and D. J. Atkinson, "Assessment of the incremental conductance maximum power point tracking algorithm," *IEEE Trans. Sustain. Energy*, vol. 4, no. 1, pp. 108–117, Jan. 2013.
[28] B. Singh and S. Sharma, "Design and implementation of four-leg voltage-source-converter-based VFC for autonomous wind energy conversion system," *IEEE Trans. Ind. Electron.*, vol. 59, no. 12, pp. 4694–4703, Dec. 2012.
[29] M. Karimi-Ghartemani, "Enhanced phase-locked loop," in *Enhanced Phase-Locked Loop Structures for Power and Energy Applications*. Hoboken, NJ, USA: Wiley, 2014, p. 250.
[30] S. A. Khajehoddin, M. Karimi-Ghartemani, A. Bakhshai, and P. Jain, "A power control method with simple structure and fast dynamic response for single-phase grid-connected DG systems," *IEEE Trans. Power Electron.*, vol. 28, no. 1, pp. 221–233, Jan. 2013.
[31] S. A. O. da Silva, P. F. Donoso-Garcia, P. C. Cortizo, and P. F. Seixas, "A three-phase line-interactive UPS system implementation with series-parallel active power-line conditioning capabilities," *IEEE Trans Ind. Appl.*, vol. 38, no. 6, pp. 1581–1590, Nov./Dec. 2002.
[32] S. A. O. da Silva, P. Donoso-Garcia, P. C. Cortizo, and P. F. Seixas, "A three-phase line-interactive UPS system implementation with series-parallel active power-line conditioning capabilities," in *Proc. 36th IAS Annu. Meeting Prod. IEEE Ind. Appl. Conf., (Cat. No.01CH37248)*, Chicago, IL, USA, 2001, vol. 4, pp. 2389–2396.
[33] G. Pathak, B. Singh, and B. K. Panigrahi, "Back-propagation algorithm-based controller for autonomous Wind–DG microgrid," *IEEE Trans. Ind. Appl.*, vol. 52, no. 5, pp. 4408–4415, Sep. 2016.
[34] B. Singh and J. Solanki, "A comparison of control algorithms for DSTATCOM," *IEEE Trans. Ind. Elect.*, vol. 56, no. 7, pp. 2738–2745, Jul. 2009.
[35] P. Kanjiya, B. Singh, A. Chandra, and K. Al-Haddad, "SRF theory revisited" to control self-supported dynamic voltage restorer (DVR) for unbalanced and nonlinear loads," *IEEE Trans. Ind. Appl.*, vol. 49, no. 5, pp. 2330–2340, Sep./Oct. 2013.

Bhim Singh (SM'99–F'10) was born in Bijnor, India, in 1956. He received the B.E. degree in electrical engineering from the University of Roorkee, India, in 1977, and earned the M.Tech. degree in power apparatus and systems and the Ph.D. degree in electrical engineering, both from the Indian Institute of Technology Delhi, India, in 1979 and 1983, respectively.

In 1983, he joined the Department of Electrical Engineering, University of Roorkee (Now IIT Roorkee) as a Lecturer. He became a Reader there in 1988. In December 1990, he joined the Department of Electrical Engineering, IIT Delhi, India, as an Assistant Professor, where he became an Associate Professor in 1994 and a Professor in 1997. He was ABB Chair Professor from September 2007 to September 2012. Since October 2012, he has been a CEA (Center Electricity Authority) Chair Professor. Currently he is also the Head of the Department of Electrical Engineering, IIT Delhi. He has guided 69 Ph.D. dissertations and 167 M.E./M.Tech./M.S.(R) theses. He has been granted one US patent and filed 25 Indian patents. He has executed more than 75 sponsored and consultancy projects. He has co-authored a text book on power quality: *Power Quality Problems and Mitigation Techniques* (Wiley, 2015). His areas of interest include power electronics, electrical machines and drives, renewable energy systems, active filters, FACTS, high voltage direct current (HVdc), and power quality.

Prof. Singh is a Fellow of the Indian National Academy of Engineering, The Indian National Science Academy, The National Academy of Science, India, The Indian Academy of Sciences, India, The World Academy of Sciences, the Institute of Engineering and Technology, Institution of Engineers (India), and Institution of Electronics and Telecommunication Engineers, and a Life Member of the Indian Society for Technical Education, System Society of India, and National Institution of Quality and Reliability.

Geeta Pathak (M'14) received the B.Tech. and M.Tech. degrees in electrical engineering from G. B. Pant University of Agriculture and Technology (GBPUA&T), Pantnagar, India, in 2003 and 2007, respectively. She received the Ph.D. degree from the Department of Electrical Engineering, I.I.T. Delhi, India, in 2017.

In March 2007, she joined the Department of Electrical Engineering, College of Technology, GBPUA&T, Pantnagar, India as an Assistant Professor. Her research interests include power electronics, wind energy conversion systems, ac microgrids, and power quality.

Bijaya Ketan Panigrahi (SM'06) received the Ph.D. degree in power systems from Sambalpur University, India, in 2004.

Since 2005, he has been an Associate Professor with the Department of Electrical Engineering, Indian Institute of Technology, New Delhi, India. Prior to joining IIT, he was a Lecturer with the University College of Engineering, Sambalpur, Orissa, for 13 years. His research interests include intelligent control of flexible ac transmission system devices, digital signal processing, power quality assessment, and application of soft computing techniques to power systems.